Performance evolution of the Nano Boron nitride enhanced bone cement composites

Hong Wang[1,2,3], Kangrui Zhang[1,2], Wenduo Niu[2], Sicong Min[1,2,3], Fan Lu[1,2,3], Shifeng Zhang[1,2,3], Wensheng Gao[4], Hua Han[1,2,3] and Yayi Xia[1,2,3]*

Abstract

Bone cement is a research hotspot and has been partially applied in the field of bone repair thanks to the good mechanical, physical and antibacterial properties. However, the easy wear and high temperature during curing characteristics would cause surrounding tissue necrosis, which seriously limits the wider application to some extent. In this work, the hexagonal boron nitride (h-BN) nano flakes were optimized to enhance the bone cement matrix (PMMA) via mechanical doping. The doping of h-BN into PMMA results in an improved mechanical (bending stress increased by 26%), thermal-conductivity (increased by 175% with the loading of 20 wt%), wear-resistance properties, in addition, the h-BN has no significant impact on cell activity. What's more, the co-modification of PMMA with h-BN and Vancomycin (Va) endows the bone cement composites with more persistent drug release characteristics. This comprehensive performance evolution evaluation provides a reference for the innovative application of modified bone cement.

Keywords Bone cement, Nano Boron nitride, Bone repair, Performance evolution

Introduction

Osteoarthritis is a common and widespread chronic degenerative joint disease. At present, the artificial joint replacement remains the gold standard for treatment of advance osteoarthritis [1], periprosthetic joint infection(PJI) is a vital factor in determining the success of the operation [2]. Previous studies have shown that two-stage revision surgery is the gold standard for the

treatment of PJI, but its core procedure is the first-stage surgical removal of the prosthesis, debridement, treatment with antibiotics bone cement placeholder to control infection [3–5]. Among them, antibiotic-loaded cement spacer was used as placeholder and shows obvious advantages. At present, bone cement with good mechanical, physical and antibacterial properties is a research hotspot in the field of bone repair [6]. Polymethylmethacrylate (PMMA) bone cement has developed rapidly in the field of Orthopaedics replying on the good biomechanical properties and shape plasticity [7]. Massimo et., al [8] analyzed 52 patients with thoracolumbar degenerative diseases with osteoporosis through a single-center observational study and found that PMMA-enhanced window opening screws can effectively treat patients who suffer from a decline in bone quality due to severe osteoporosis. Siyi et., al [9] applied bone cement osteoplasty to two patients with spinal metastatic pheochromocytoma in the spine and found that bone cement osteoplasty could

*Correspondence:
Yayi Xia
xiayayilzu@sina.com
[1]Department of Orthopaedics, Lanzhou University Second Hospital, Lanzhou, China
[2]Orthopaedics Key Laboratory of Gansu Province, Lanzhou University Second Hospital, Lanzhou University, Lanzhou, Gansu 730000, China
[3]Gansu Intelligent Orthopedics Industry Technology Center, Lanzhou, China
[4]Key Laboratory for Magnetism and Magnetic Materials of the Ministry of Education, School of Materials and Energy, Lanzhou University, Lanzhou, Gansu 730000, China

successfully treat spinal metastatic pheochromocytoma in the spine. This method could relieve pain of patients, inactivate the body's neuroendocrine system, reduce perioperative blood loss, and stabilize the spine.

Despite the successful cases mentioned above, some obvious drawbacks of PMMA bone cement [10], such as easy wear and high temperature during curing, results in the surrounding tissue is prone to necrosis [11, 12], long-term use is prone to fracture [13] and loosening [14]. Simultaneously, the duration of antibiotic release within antibiotic-loaded bone cement is limited, and the quantity of released antibiotics is minimal [15, 16]. These characteristics make its wide application to be limited to some extent. As we all know, the polymer nano-composites achieve the "cutting", "matching", and "assembly" of their functions by leveraging the morphology, structure, and size effects of nanofillers, as well as the synergistic effect between nanofillers and polymer matrices [17], endowing polymers with special functionalities and improved intrinsic properties [18]. Which inspires us to improve the weakness of bone cement via nano filler reinforcing strategy.

In recent years, boron nitride with graphite-like structure has become a research hotspot in nano filler materials, and shows prospective applications in the medical materials due to the excellent chemical stability, strong corrosion resistance and physical properties [19]. Especially, large amounts of h-BN doping PMMA works indicate that the h-BN obviously improve the thermal diffusion coefficient of the PMMA matrix [20–22], which shows potential to deal with the problem of high-temperature tissue necrosis relying on the improved thermal conductivity of the matrix. In addition, the nano h-BN could obviously improve the wear resistance [23, 24] and mechanical properties [25, 26] of the polymer composites relying on the two-dimensional structure and intrinsic properties. Therefore, above features from h-BN doping are expected to solve the problems caused form easy wear and high temperature during curing for the bonce cement matrix. In addition, nanomaterials can serve as drug carriers [27] can assist in navigating transporting barriers, and can effectively control drug release and improve drug efficacy. Herein, in this work, the h-BN nano flakes were employed to enhance the bone cement matrix via a mechanical mixing. The optimized h-BN/PMMA composites display the improved thermal conductivity, wear-resistance, antibacterial and drug release properties. The co-doping of nano h-BN flakes and functional drugs provides an effective strategy for improving the postoperative side effects of bone repair, contributing from the synergistic effects between the functions of various components.

Methods

Preparation of h-BN nano flakes

The h-BN nanoflakes were synthesized through an efficient ball milling method.[20] Specifically, 5 g of micron-sized h-BN powder were combined with a 2 M NaOH solution in a steel grinding bowl, maintaining a ball-to-powder ratio of 20:1. The mixture was then subjected to a rotational speed of 300 rpm for 18 h, facilitating the exfoliation of h-BN into nanoflakes. Following this, the exfoliated nanoflakes were carefully collected and subjected to a washing process with HCl solution to eliminate metallic impurities. Subsequently, they were rinsed thoroughly with deionized (DI) water until the pH reached neutrality, close to 7. Finally, the purified samples were dried to completion.

Preparation of composite bone cement

The h-BN/PMMA + Va composites were processed by mechanical compounding through a Lab Tech mixer at 28 °C. Briefly, Bone cement (PALACOS R + G) is composed of a powder (48 g, main constituent of poly (methyl acrylate, methyl methacrylate), methyl methacrylate and little benzoyl peroxide, zirconium dioxide, gentamicin base (as sulphate)) and liquid package (20 mL, main constituent of methyl methacrylate and little NN-dimethyl-p-toluidine). The powder was firstly mixed with designed h-BN/vancomycin, and poured into a sterilized mechanical mixer, subsequently, the liquid is added. Subsequently, the mixture was meticulously stirred for 30 s until a dough-like consistency was achieved, at which point it ceased adhering to the mechanical rotor. The dough was pressed into flat samples ($10 \times 10 \times 1.2$ mm^3) for further processing. The samples were named as x wt%-hBN/PMMA + Va according to the h-BN loading, the x is the doping mass percentage.

Characterization

The phase structures of h-BN and h-BN/PMMA + Va composites were precisely determined using X-ray diffraction (XRD, Rigaku D/max-2400). The surface morphology and wear surface structure of the h-BN nanoflakes and h-BN/PMMA + Va composites were thoroughly characterized via scanning electron microscopy (SEM, Apreo S). Fourier transform infrared (FTIR) spectroscopy was employed to collect spectra on a Nicolet NEXUS 670 instrument, spanning a wavelength range from 4000 to 400 cm^{-1}. Thermal conductivity measurements were conducted on an LFA1000 Laser Thermal Diffusion/Thermal Conductivity Tester, utilizing samples with a diameter of 8 mm. The mechanical properties of PMMA and the composite were evaluated using the 6501 desktop material testing machine from MTS, located in the United States. The tribological properties of the h-BN/PMMA + Va composites were analyzed in a

reciprocating mode on a tribometer (TRB3, Anton Paar, Netherlands). The test conditions included a reciprocating distance of 2 mm, a frequency ranging from 1 to 5 Hz, a load of 1 N, 4500 test cycles, and a temperature of 25 °C. The coefficient of friction (COF) was automatically recorded by a computer system connected to the tribometer. Following the test, the wear volume was calculated using the cylinder calculation equation. The tribological performance was performed on a universal mechanical tester (UMT-3, Bruker) in ball-on-disk contact mode. A GCr15 steel ball (diameter = 3 mm) was selected as the counterpart. The wear rate of all samples was calculated as follows: Wear rate = V/PL. Themicro-hardness of the samples was investigated by Vickers hardness measurement technique using Vickers hardness tester (ZHV30 Z, wick/Roell, Germany).

Antibacterial performance testing

During the experiment, staphylococcus aureus (S. aureus) (ATCC 29213) was cultured in the LB medium at 37 °C for 24 h. Take an appropriate amount of mature bacterial colonies and incubate them in 10 ml TSB liquid medium at 37 ℃ for 6–8 h, reaching an OD600 of about 0.6. After adjusting to 0.6 with TSB, dilute 100 times to 1.5×10^7 cfu, and co culture 5 ml of bacterial solution with the material. Incubate at 37 ℃ for 24 h. Collect bacterial liquid on the surface of the material and dilute it in gradient: Take several centrifuge tubes labeled with numbers 1-n, add 900 μL of physiological saline to each

tube, take 100 μL of the original solution and add it to tube 1, which is a 10 folds dilution solution. After mixing, take 100 μL from tube 1 and add it to tube 2. Dilute it sequentially to tube n, and then take 100 μL of the liquid from appropriate dilution gradient tubes and apply it to the TSA plate. Incubate at 37 ℃ for 18 h and take photos for counting. Select one suitable dilution gradient for each group to calculate the antibacterial rate, which was counted via fully automatic colony counter (Interscience, SCAN1200).

Biological properties

In vitro cellular assays were performed by osteoblas cell line (MC-3T3) [28] according to ISO 10,993 – 1994 to evaluate the biological properties of bone cements(ISO 10993-11:1994, Biological evaluation of medical devices-Part 11:Tests for systemic toxicity.2003.). For culture of MC-3T3 cell line, DMEM medium containing 10% FBS and 1% penicillin-streptomycin was prepared. MC-3T3 cell was incubated in a constant temperature incubator of 5% CO2 at 37 °C. The samples were exposed to ultraviolet light for 30 min and soaked in complete medium. Five different concentrations of diluents which 385 mg/ml(100%), 192.5 mg/ml(50%), 96.25 mg/ml(25%), 48.125 mg/ml(12.5%) and 24.0625 mg/ml(6.25%) were prepared. The study was divided into 37 groups: control group(cell culture medium), samples of different concentrations and blank group. Then, the cells were subcultured or used for the cell viability assays. The above samples were soaked in the proportion of 0.2 g/mL for 24 h to prepare the extract. The effect of bone cement on the proliferation of MC3T3 cells was detected by MTT method. The cells were inoculated in 96-well plate at the density of 4×10^3-well. After the cells were attached, PBS extract was added respectively. 10 μL CCK-8 solution was added to each well at 1d, 3d, 5d and 7d, respectively, and incubated at 37℃ for 2 h in 5%CO2 incubator. the ELISA reader was used to measure the light absorption at 450 nm. The (OD control) represents the average optical density measured for untreated cells across three plates, whereas (OD treated) signifies the mean optical density recorded for treated cells in three separate plates.

$$Cytotoxicity\% = \frac{(OD_{control} - OD_{treated})}{OD_{controal} \times 100}$$

Results and discussions

X-ray diffraction (XRD) pattern of h-BN displays an obvious characteristic peak that centered at 26.8º and 41.6 º, which are assigned to the (002) and (100) crystalline planes of h-BN (PDF# 34–0421), respectively (Fig. 1a). The additive zirconium dioxide in PMMA shows three sharp characteristic peaks that centered at
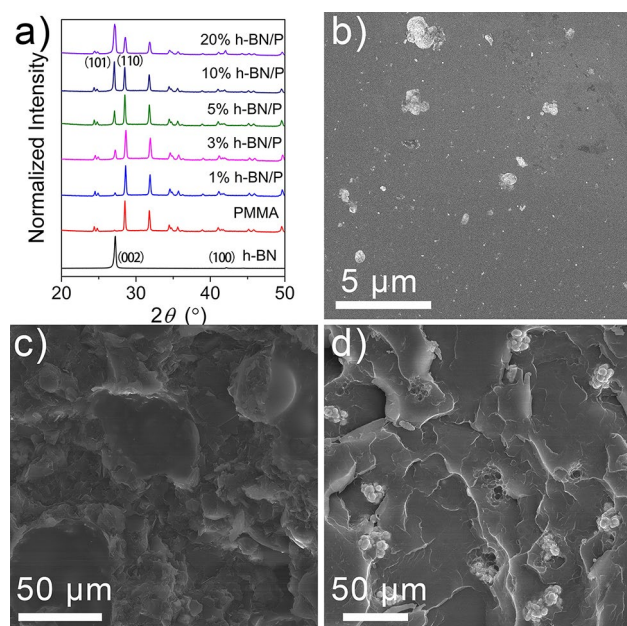

Fig. 1 Structure characterization. The XRD patterns (**a**) and SEM images of the pure h-BN (**b**), SEM micrograph of fractured surface of PMMA (**c**) and SEM micrograph of fractured surface of based nanocomposite containing 3wt.% h-BN/PMMA nanocomposites (**d**)

34.9º, 40.5º [29], assigned to the (101) and (110) crystalline planes. With the increasing of the h-BN percent in PMMA matrix, the characteristic peak of h-BN on XRD patterns gradually becomes stronger without the changing of the phase structure and shifting of characteristic peak of PMMA, which demonstrates that the h-BN was uniformly dispersed into the PMMA matrix and didn't change the crystalline structure of the PMMA. The scanning electron microscopy (SEM) graphic shows the pure h-BN own a smooth layered structure (Fig. 1b), after compounding into the PMMA matrix, compared to pure PMMA (Fig. 1c), As evident in Fig. 1d, the h-BN exhibits a remarkably uniform dispersion within the PMMA matrix, resulting in a neater and smoother cross-section of the h-BN/PMMA composite.

The changes in the component properties of h-BN modified PMMA composite are further investigated via FT-IR. The graph prominently displays strong absorption peaks at 1370 cm⁻¹ and 805 cm⁻¹, as depicted in Fig. 2. These peaks correspond to the in-plane stretching vibration and out-of-plane bending vibration of B-N bonds, respectively [30]. There is no obvious peak on the h-BN FT-IR spectra, indicating the complete structure and clean surface. After incorporated into the PMMA matix, the characteristic peaks of the h-BN gradually increased with the increasing of the h-BN loadinds, indicating a unifrom dispersion of the h-BN in bone cement matix, which agrees well with the XRD and SEM results.

The mechanical properties of h-BN/PMMA + Va composites were tested via the Instron testing system shown in Fig. 3. After mixing the Va and h-BN, the bending strength of the composites gradually decreases with the

Fig. 2 FT-IR spectra of h-BN, PMMA, and h-BN doping PMMA composites

increasing of the h-BN content (Fig. 3a). The fracture bending stress shows a slightly increase when the h-BN loading is 1wt.%, but the whole trend is similar with the changing of bending strength (Fig. 3b). The flexural modulus (Fig. 3c) and bending stress (Fig. 3d) show a typical "volcanic trend" with the changing of the h-BN doping content, the 1wt.%-hBN/PMMA displays the maximized mechanical property. Above results demonstrate the h-BN nano flakes perform the significant improvement in the modulus and stress, showing an obvious nano-enhancing effect at a low content doping. When the loadings of h-BN further increasing, the mechanical properties of the PMMA matrix would obviously decreased due to the sacrifice of polymer structural performance [31].

To assess the abrasion resistance of h-BN doped PMMA composites, the following experimental procedure was adopted for all prepared samples. Abrasion tests were conducted using a Taber model 5130 abrader, with sample specimens measuring $1 \times 10 \times 10$ mm³. The samples underwent 5000 cycles of abrasion testing. As shown in Fig. 4a, the pure PMMA presents a relatively low friction coefficient, as the increasing of h-BN loading, the friction coefficient of the composites shows a trend of first increasing and then decreasing. But the wear rate of the composites gradually decreased with the increasing of h-BN loading (Fig. 4b), which was evaluated as the loss of sample weight. As obviously observed, the presence of nano h-BN particles obviously improves wear resistance [32]. To investigate this evolution mechanism, the wear marks were analysis via SEM characterization. As show in Fig. 4c, under a low h-BN loading of 1 wt%, the presence of nanoparticles increases the resistance to the probe, which may cause an increase of friction coefficient. With the adding of h-BN nanoparticles loadings in PMMA matrix, the surface wear marks gradually become smooth, gradually reflecting the properties of boron nitride continuous phase, which is reflected in the test data as the friction coefficient gradually decreases after reaching its peak, while the wear resistance gradually increases. Above results demonstrates that the doping of h-BN nano flakes into PMMA matrix can significantly improve the wear resistance. The VH hardness values of 3%-h BN/P reached 1625 MPa, which increased by 90% compared to pure PMMA (854 MPa).

To investigate the interface heat release performance of the bone cement composites, As depicted in Fig. 5, the thermal conductivity tests were conducted on samples with a thickness of 2 mm. At low h-BN loadings, minimal impact on the thermal conductivity of the composites was observed. However, a notable increase in thermal conductivity was achieved with the incorporation of 5–10 wt% of h-BN, indicating the significant contribution of h-BN to enhancing thermal conductivity. As reflected
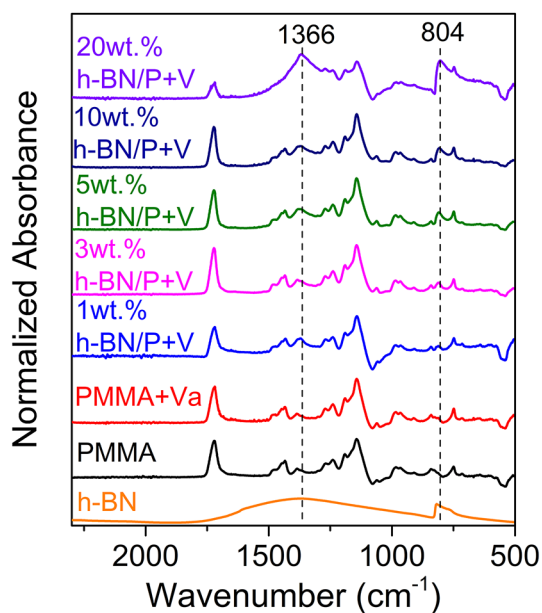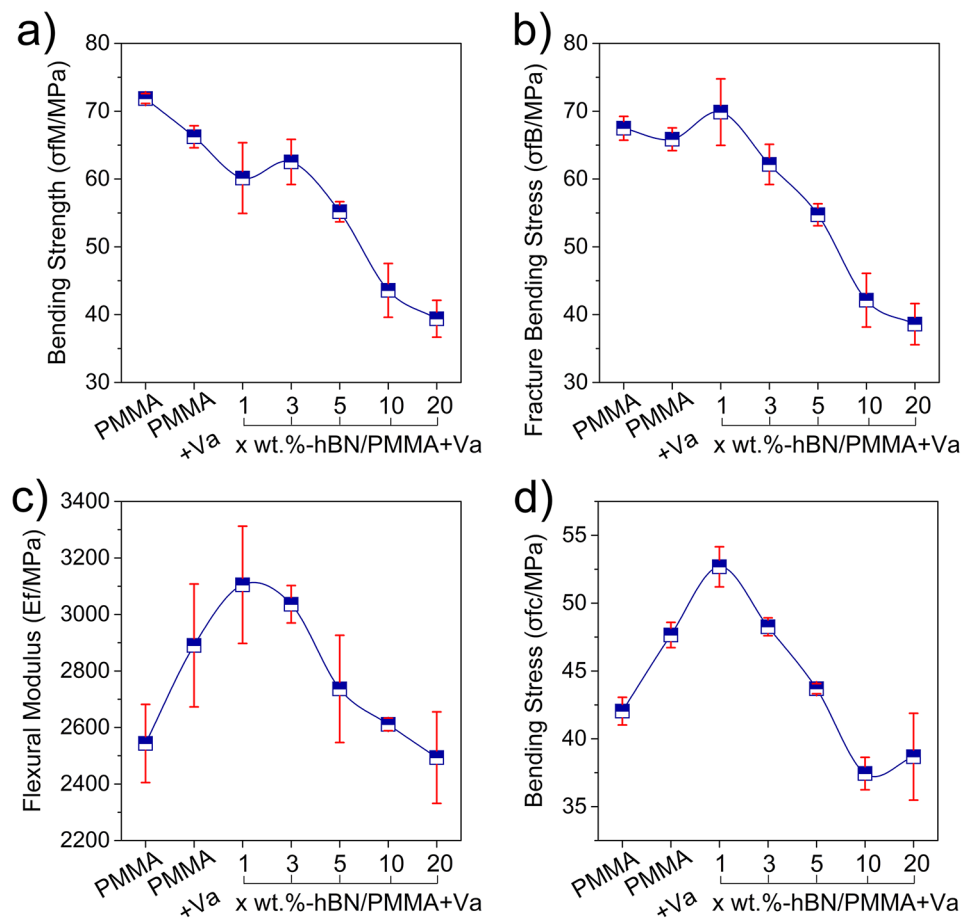
Fig. 3 The mechanical test of the composites and control samples. (**a**) Bending strength; (**b**) Fracture bending strength; (**c**) Flexural modulus; (**d**) Bending stress. Repeat the sample testing five times for all samples according to ASTM D7264 standard

in previous work, the improved thermal conductivity is originated from the high thermal stability and thermal conductivity of BN [33, 34]. This obviously enhanced thermal conductivity for the bone cement composites is undoubtedly a very favorable signal for alleviating or even solving the problem of peripheral tissue necrosis caused by local high temperature during curing.

Figure 6 illustrates the antibacterial activities of both control and nanocomposite samples, as assessed through a disc-diffusion test against E. coli bacteria after a 24-hour incubation period. As clearly demonstrated in Fig. 6 (insert image), the inhibition zone dimeter is 14.4 mm for pure PMMA sample, after adding Va into PMMA, the inhibition zone dimeter increased to 28.7 mm with a growth of 99%, demonstrating that the Va in PMMA matrix retain an excellent antibacterial property. When the h-BN nanosheets were mixed with Va and compounded into PMMA, the inhibition zone dimeter of the 1.wt% h-BN/PMMA + Va composites further increased to 30.4 mm, all the composites with different h-BN doping ratio displays no decrease at all, indicating the antibacterial activity induced by h-BN nanosheets [35]. In addition, the increased inhibition zone of h-BN doped PMMA + Va composites also reflects the continuous drug release ability compared with PMMA + Va sample.

To investigate the biocompatibility and potential cytotoxicity of h-BN doped PMMA + Va composites, an in vitro study was conducted utilizing an MTT assay. This assay aimed to evaluate the response of cultured osteoblas cells to the nanocomposites, providing insights into their safety for biomedical applications. Figure 7 shows the results of co culture of h-BN doping PMMA composites in different concentrations. As shown in Fig. 7a the high concentrations, there was no significant difference in the cell proliferation rate of PMMA composites on the first day compared to the control group. With time increasing, the cell proliferation rate of all samples gradually decreases, however, the h-BN doped PMMA samples all display the higher cell proliferation rate compared to the non-doped PMMA, which indicates the doping of nano h-BN is beneficial for improving the biocompatibility of the PMMA matrix. Simultaneously, as shown in Fig. 7b, the cell proliferation rate of PMMA is close to 99% at all detection concentrations in the first day,
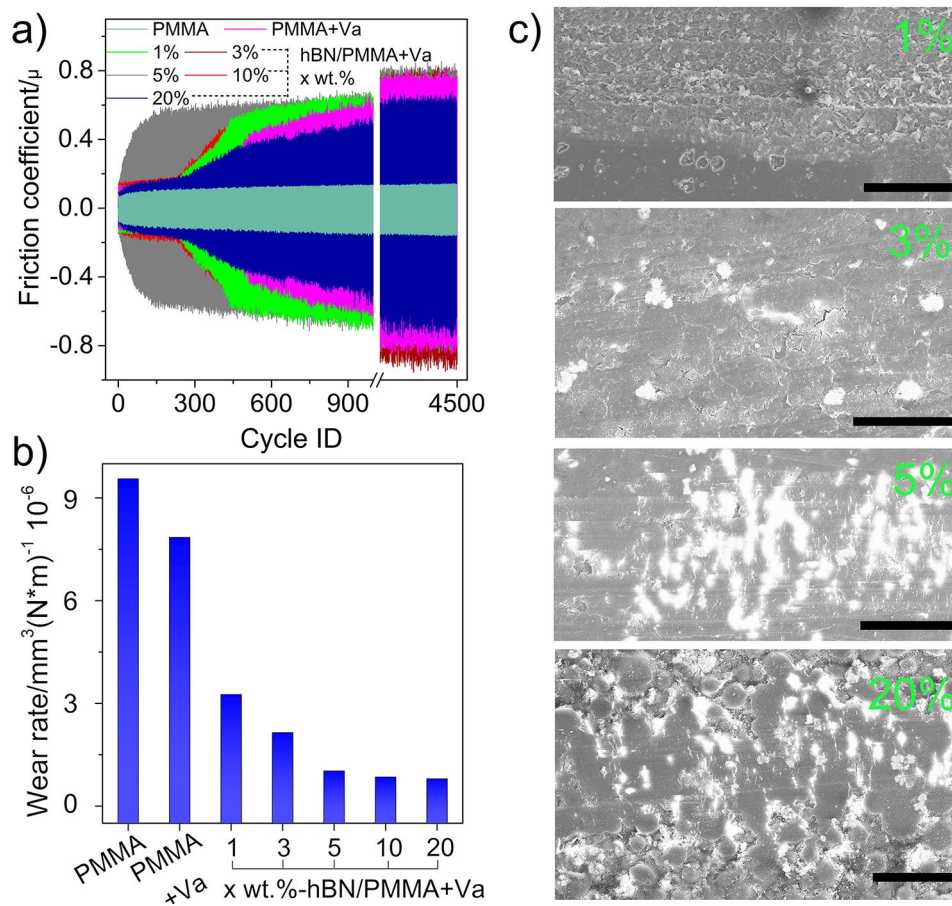
Fig. 4 The COF curve of the composites and control samples from the first to the 4500th time; (**b**) Ware rates; (**c**) SEM micrographs of worn surfaces of h-BN/PMMA composites with different loadings, tested under the load of 1 N. the scale bar is 200 μm
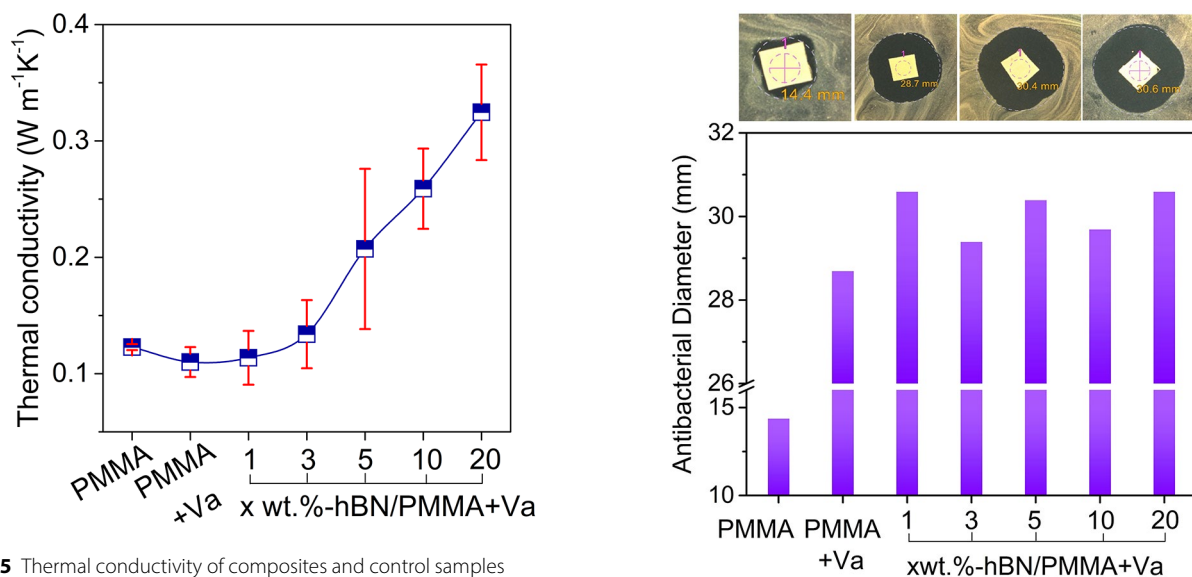

Fig. 5 Thermal conductivity of composites and control samples

Fig. 6 Antibacterial activity of control and nanocomposite samples with different ratios against E. coli. Bacteria. The photos from left to right are designed to PMMA, PMMA+Va, 3 wt%-hBN/PMMA+Va and 10 wt%-hBN/PMMA+Va, respectively

indicating that the PMMA and h-BN doping PMMA are non-toxic at low concentrations and exhibit the good biocompatibility [36, 37]. With the further extension of evaluation time (Fig. 7c and d), all composites exhibited
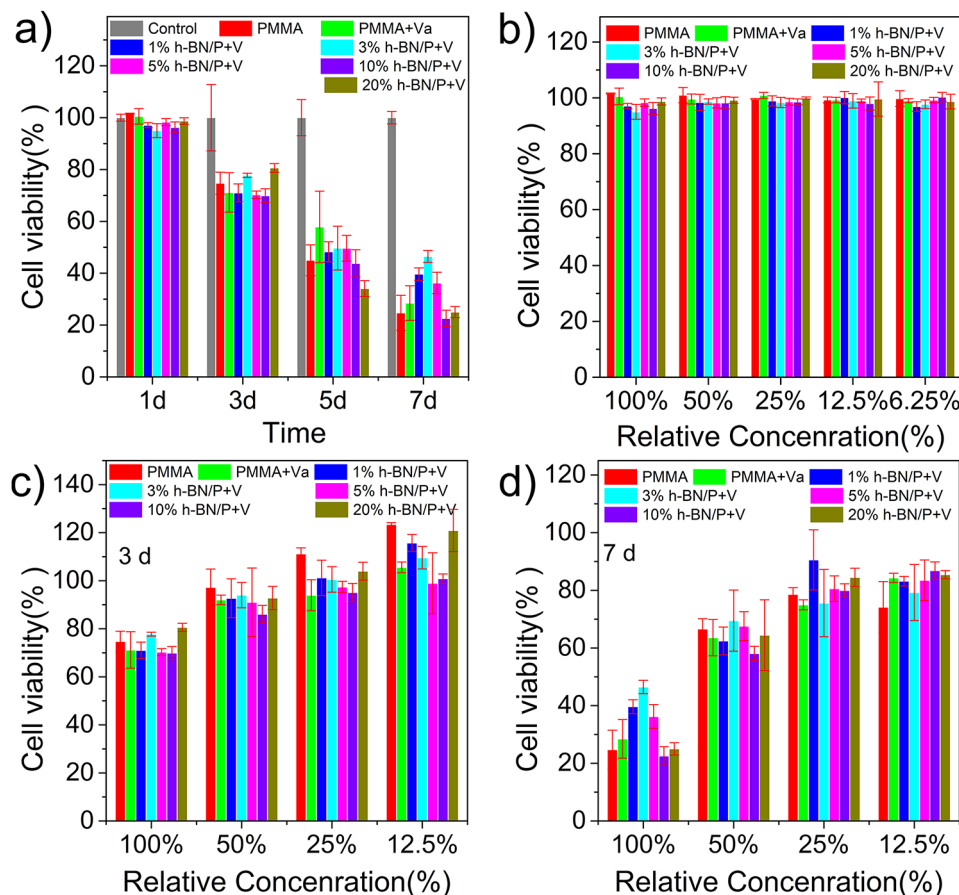
Fig. 7 Cytotoxicity assay of PMMA and PMMA composites versus different h-BN loadings in 100% relative concentration (**a**); Cytotoxicity assay of PMMA and h-BN/PMMA composites versus concentration in different time of 1d (**b**); 3d (**c**) and 7d (**d**)

a gradually increased cell proliferation rate with the decreasing of relative concentration, it's noted, the h-BN doped PMMA samples all show much higher cell proliferation rate than the non-doped PMMA control samples, demonstrating the enhancing effect of the nano h-BN. The low toxicity and good biocompatibility of PMMA and h-BN doped PMMA provide an effective theoretical basis for their use as biomedical materials.

Conclusion

In this work, the h-BN nano flakes and Va was co-doped into the PMMA matrix via a mechanical mixing in RT. The composites demonstrate improved physical and biological properties, especially the enhanced wear-resistance and thermal conductivity, which is expected to improve the problem of surrounding tissue necrosis as a result from the easy wear and high temperature during curing characteristics. Besides, the high biocompatibility and enhanced drug release characteristics of h-BN/PMMA + Va composite lays a theoretical foundation for its further clinical application. This multifunctional collaborative strategy provides new route for improving the performance of medical materials.

Author contributions
(I) Designed and performed: Yayi Xia, Hua Han, Wensheng Gao; (II) Performed Test: Hong Wang, Wenduo Niu, Wensheng Gao, Sicong Min; (III) Manuscript writing, assembly of data and interpretation: Hong Wang, Kangrui Zhang, Wensheng Gao; (IV) Cell culture and Cytotoxicity assay: Hong Wang, Kangrui Zhang, Wenduo Niu; (V) mechanical test and collection of data: Sicong Min, Shifeng Zhang, Fan Lu; (VI). All authors read and approved the final manuscript.

Data availability
No datasets were generated or analysed during the current study.

Declarations

Ethics approval and consent to participate
No ethical experiments were involved in this study.

Consent for publication
All authors gave their consent for this study to be published.

Competing interests
The authors declare no competing interests.

References
1. McCalden RW, et al. Comparison of outcomes and survivorship between patients of different age groups following TKA. J Arthroplasty. 2013;28:83–6.
2. Namba RS et al. Risk factors associated with deep surgical site infections after primary total knee arthroplasty: an analysis of 56,216 knees. J Bone Joint Surg Am. 2013(95):775–82.
3. Kunutsor SK, et al. Re-Infection outcomes following One- and Two-Stage surgical revision of infected knee prosthesis: A systematic review and Meta-Analysis. PLoS ONE. 2016;11:e0151537.
4. Ghanem E, et al. Staged revision for knee arthroplasty infection: what is the role of serologic tests before reimplantation? Clin Orthop Relat Res. 2009;467:1699–705.
5. Postler A et al. Analysis of total knee arthroplasty revision causes. BMC Musculoskelet Disord. 2018(19)55.
6. Bai M et al. Application of PMMA bone cement composited with bone-mineralized collagen in percutaneous kyphoplasty. Regen Biomater. 2017(4):251–5.
7. López A, et al. Direct and interactive effects of three variables on properties of PMMA bone cement for vertebral body augmentation. J Mater Sci Mater Med. 2011;22:1599–606.
8. Girardo M, et al. Surgical treatment of osteoporotic thoraco-lumbar compressive fractures: the use of pedicle screw with augmentation PMMA. Eur Spine J. 2017;26:546–51.
9. Cai S et al. Successful treatment of metastatic pheochromocytoma in the spine with cement augmentation. Med (Baltim). 2017(96)e5892.
10. Lopez-Heredia MA, et al. Bulk properties and bioactivity assessment of porous polymethylmethacrylate cement loaded with calcium phosphates under simulated physiological conditions. Acta Biomater. 2012;8:3120–7.
11. Sugino A, et al. Relationship between apatite-forming ability and mechanical properties of bioactive PMMA-based bone cement modified with calcium salts and alkoxysilane. J Mater Sci Mater Med. 2008;19:1399–405.
12. Golz T, et al. Temperature elevation during simulated polymethylmethacrylate (PMMA) cranioplasty in a cadaver model. J Clin Neurosci. 2010;17:617–22.
13. Yamada M, et al. Current bone substitutes for implant dentistry. J Prosthodont Res. 2018;62:152–61.
14. Schunck A, et al. Release of zirconia nanoparticles at the metal stem-bone cement interface in implant loosening of total hip replacements. Acta Biomater. 2016;31:412–24.
15. Anagnostakos K, et al. Enhancement of antibiotic elution from acrylic bone cement. J Biomed Mater Res B Appl Biomater. 2009;90:467–75.
16. Carli AV, et al. Vancomycin-Loaded polymethylmethacrylate spacers fail to eradicate periprosthetic joint infection in a clinically representative mouse model. J Bone Joint Surg Am. 2018;100:e76.
17. Sivaramakrishnan S, et al. Controlled insulator-to-metal transformation in printable polymer composites with nanometal clusters. Nat Mater. 2007;6:149–55.
18. Gao W, et al. Architecture & functionalization evolution of RGO affect physicomechanical properties of Polyolefin/RGO composites. Compos Part a-Applied Sci Manuf. 2018;107:479–88.
19. Liu Z et al. Ultrathin high-temperature oxidation-resistant coatings of hexagonal Boron nitride. Nat Commun. 2013(4):2541.
20. Su K-H et al. Development of thermally conductive polyurethane composite by low filler loading of spherical BN/PMMA composite powder. Sci Rep. 2019(9)14397.
21. Tang Y, et al. Synergetic enhancement of thermal conductivity in the silica-coated Boron nitride (SiO2@BN)/polymethyl methacrylate (PMMA) composites. Colloid Polym Sci. 2020;298:385–93.
22. Zhi CY, et al. Mechanical and thermal properties of polymethyl Methacrylate-BN nanotube composites. J Nanomaterials. 2008;2008:642036.
23. Yu J, et al. Tribological properties of epoxy composite coatings reinforced with functionalized C-BN and H-BN nanofillers. Appl Surf Sci. 2018;434:1311–20.
24. Harichandran R, et al. Microstructure and mechanical characterization of (B4C + h-BN)/Al hybrid nanocomposites processed by ultrasound assisted casting. Int J Mech Sci. 2018;144:814–26.
25. Li R et al. Porous Boron nitride nanofibers/pva hydrogels with improved mechanical property and thermal stability. Ceram Int. 2018(44).
26. Jing L, et al. Biocompatible hydroxylated Boron nitride Nanosheets/Poly(vinyl alcohol) Interpenetrating Hydrogels with Enhanced Mechanical and Thermal Responses. ACS Nano. 2017;11:3742–51.
27. Hubbell JA, et al. Nanomaterials for drug delivery. Science. 2012;337:303–5.
28. Al-Shammari AM et al. Newcastle disease virus, rituximab, and doxorubicin combination as anti-hematological malignancy therapy. Oncolytic Virother. 2016(5):27–34.
29. Reddy CV, et al. Synthesis and characterization of pure tetragonal ZrO2 nanoparticles with enhanced photocatalytic activity. Ceram Int. 2018;44:6940–8.
30. Wu K et al. Preparation of a thermally conductive biodegradable cellulose nanofiber/hydroxylated Boron nitride nanosheet film: the critical role of edge-hydroxylation. J Mater Chem A. 2018(6):11863–73.
31. Gao W et al. Performance evolution of alkylation graphene oxide reinforcing High-Density polyethylene. J Phys Chem C. 2017(121):21685–94.
32. Chen J, et al. Mechanical and tribological properties of h-BN/ZrO2/SiC solid-lubricating ceramic composites. Tribol Int. 2021;160:107061.
33. Lu Y, et al. Boron nitride self-assembly cladding structure promoting thermal property and dimensional stability of polymer composites. Compos Sci Technol. 2021;201:108536.
34. Kong L et al. Constructing integrated thermal conductive and flame-retardant filler network in ceramifiable epoxy composites. J Reinf Plast Compos. 202307316844231198303.
35. Phakatkar AH, et al. Novel PMMA bone cement nanocomposites containing magnesium phosphate nanosheets and hydroxyapatite nanofibers. Mater Sci Engineering: C. 2020;109:110497.
36. Bulut O, et al. Catalytic evaluation of biocompatible chitosan-stabilized gold nanoparticles on oxidation of Morin. Carbohydr Polym. 2021;258:117699.
37. Saeedi Garakani S, et al. Fabrication of Chitosan/agarose scaffolds containing extracellular matrix for tissue engineering applications. Int J Biol Macromol. 2020;143:533–45.

Publisher's note
Springer Nature remains neutral with regard to jurisdictional claims in published maps and institutional affiliations.